We are IntechOpen,
the world's leading publisher of
Open Access books
Built by scientists, for scientists

6,900
Open access books available

186,000
International authors and editors

200M
Downloads

Our authors are among the

154
Countries delivered to

TOP 1%
most cited scientists

12.2%
Contributors from top 500 universities

CLARIVATE ANALYTICS
BOOK CITATION INDEX
INDEXED

WEB OF SCIENCE™

Selection of our books indexed in the Book Citation Index
in Web of Science™ Core Collection (BKCI)

Interested in publishing with us?
Contact book.department@intechopen.com

Numbers displayed above are based on latest data collected.
For more information visit www.intechopen.com

Design Considerations for Magnetically Actuated Biomimetic Cilia

Benjamin Evans[1] and Rich Superfine[2]
[1]Elon University
[2]University of North Carolina at Chapel Hill
USA

1. Introduction

Biology has produced extraordinary solutions for functions necessary for life. Sensing and movement appear to be two such necessary functions. For both of these, biology has developed extensions from the cell body called cilia (Sleigh, 1962). For movement – either of the entire organism or for moving fluid and hence nutrients toward the stationary organism – nature has evolved motile cilia (Satir, Mitchell, & Jekely, 2008). These remarkable structures, consisting of a highly organized collection of several hundred thousand proteins packed in a single 250 nanometer diameter cylinder 7 microns long, beat in regular bend shapes autonomously, fuelled by chemical energy (Nicastro, 2009; Satir & Christensen, 2007). Cilia exist throughout biology, from single cell organisms to humans, and are essentially identical down to the protein level across this vast range of life forms. Within the human body, the literature on their significance to human health has exploded over the past decade (Cardenas-Rodriguez & Badano, 2009). Cilia have long been understood to be the critical mechanism for fighting lung infections through the propulsion of mucus (Antunes & Cohen, 2007; Boucher, 2007). More recently, cilia have been found to guide neurons within the brain and to be responsible for the left-right asymmetry of the human body (Okada & Hirokawa, 2009; Sutherland & Ware, 2009). Whether for organism propulsion or for its more complex physiological functions, the cilium is the primary manner in which the cell interacts with surrounding fluids (Cartwright, Piro, Piro, & Tuval, 2008; Smith, Gaffney, & Blake, 2009). Each of these issues: the structure, operation and function of cilia remains a major challenge for biological physics. Difficult unanswered questions remain in the protein-level organization of the cilium, the coordination of 4000 molecular motors to produce bend shapes and the structure-fluid interaction of beating, slender bodies with Newtonian and viscoelastic fluids.

From an engineering perspective, cilia present a challenge for replicating their function at the micrometer length scale. Applications of such structures may include microfluidics for pumping and mixing, sensing surfaces for measuring local fluid flows and active surfaces for energy applications and the inhibition of biofouling. We are far from having the ability to replicate the extraordinary, nanoscale architecture of the cilium. However, we have been successful recently at replicating the functional capability of cilia at the sub-micron length scale through a variety of advances in materials and fabrication strategies. We begin our discussion with magnetic materials as magnetic actuation offers flexibility in design and

application to arrays of moving structures. With candidate materials in hand, we then describe fabrication strategies that permit well defined, highly elongated structures in large area arrays. We need to actuate these structures with bend shapes appropriate for moving fluids. We therefore describe the physics of the magnetic actuation of extended structures, including specific field generation schemes and the bend shapes that result. Throughout these sections we present general guidelines for the design space within which an engineer would operate.

While biology provides inspiration for engineering solutions, the resulting technology allows us to reflect an engineering understanding back onto biological design challenges. We therefore end this review with a discussion of the overall hydrodynamic, energy and force considerations that the biological cilia are designed to solve and compare our technical achievement with the remarkable molecular solution of biology. It will not surprise the reader that we remain in awe of the nanotechnology of life.

2. Materials

2.1 Introduction

The ideal material for a magnetic microactuator must be both flexible and magnetic. In any single material, these qualities are generally mutually exclusive. Magnetic materials are with rare exception metallic, and therefore of high modulus while soft polymeric materials may exhibit only a slight diamagnetism. We can, however, combine the flexibility of a polymer with the magnetization of a metal by developing a composite material in which magnetic particles are suspended within a polymer matrix. Depending on their modulus, such materials are referred to as either ferrogels (soft) or magnetic elastomers (firm). In this work, we will use the latter term to refer to both.

2.2 Nanoparticle candidates

Magnetic elastomers first began to appear in the literature about 20 years ago, and a wide range of such materials have now been described. The vast majority of these materials use iron oxide nanoparticles as their magnetic component (either magnetite: Fe_3O_4, or maghemite: Fe_2O_3), since procedures for their fabrication are simple and well-established (Bee, Massart, & Neveu, 1995; Massart, 1981; Massart, Dubois, Cabuil, & Hasmonay, 1995; van Ewijk, Vroege, & Philipse, 1999). The room temperature saturation magnetizations of 480 kA/m for magnetite and 380 kA/m for maghemite differ by a relatively small proportion (Dunlop & Ozdemir, 1997). While a few materials use cobalt nanoparticles or alloys of cobalt, iron, and nickel, saturation magnetizations of such materials are generally on par with those for iron oxides, and therefore the most significant factor in the magnetization of a composite material is not the choice of nanoparticle but the loading fraction of particles within the matrix.

Magnetic elastomers containing magnetite or maghemite nanoparticles are by far the most prevalent in the literature, and therefore calculations in this work will generally consider the loading material to be maghemite. Magnetization of maghemite nanoparticles as a function of applied field is shown in Fig. 1, below. Synthesis of stable aqueous solutions of iron oxide nanoparticles under acidic or alkaline conditions was first described by Massart (Massart, 1981), and such solvents are stable up to a concentration of about 5% nanoparticles by weight. These solutions can be made stable at higher concentrations at neutral pH with the addition of sodium citrate and tetramethylammonium hydroxide, or may be transferred to

an organic phase (Dubois, Cabuil, Boue, & Perzynski, 1999; van Ewijk et al., 1999). The former is particularly useful in the synthesis of hydrogel-based magnetic elastomers which are often crosslinked under conditions of controlled pH, while the latter renders particles suitable for a hydrophobic matrix.
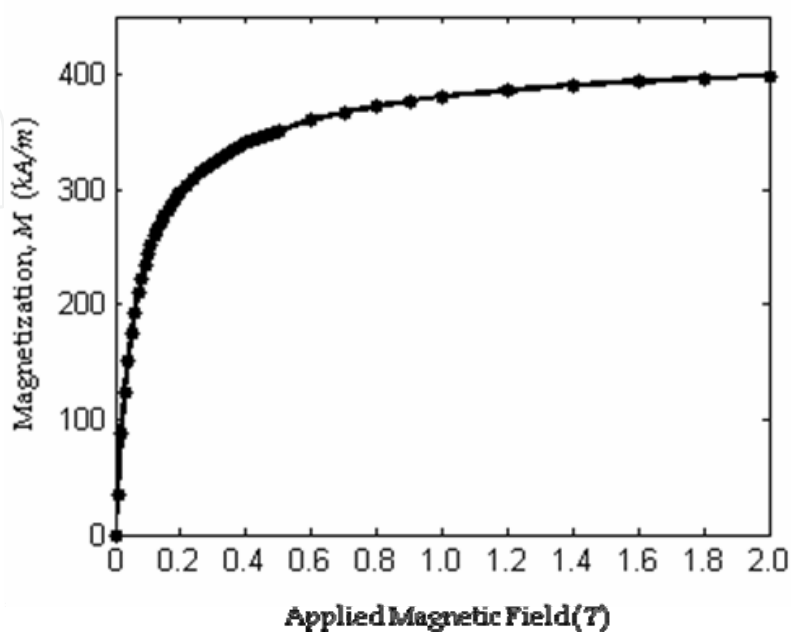

Fig. 1. Room-temperature magnetization of maghemite nanoparticles as a function of applied magnetic field, by our own SQUID measurements.

2.3 Polymer candidates

As for the polymer matrix, the most common choices by far are soft, hydrophilic magnetic elastomers such as those constructed of polyacrylamide (Caykara, Yoruk, & Demirci, 2009; Galicia et al., 2003; Mayer, Cabuil, Lalot, & Thouvenot, 2000), N-isopropylacrylamide (Xulu, Filipcsei, & Zrinyi, 2000), polyvinyl alcohol (Barsi, Buki, Szabo, & Zrinyi, 1996; Collin, Auernhammer, Gavat, Martinoty, & Brand, 2003; H. Lin, Watanabe, Kimura, Hanabusa, & Shirai, 2003; Mitsumata et al., 1999; Resendiz-Hernandez, Rodriguez-Fernandez, & Garcia-Cerda, 2008; Szabo, Czako-Nagy, Zrinyi, & Vertes, 2000; Zrinyi, Barsi, & Buki, 1997), and their derivative copolymers (C. L. Lin, Chiu, & Don, 2006). Also prevalent are gelatin (Saslawski, Weingarten, Benoit, & Couvreur, 1988) and copolymers of polyethylene oxide (Qin et al., 2009; Wormuth, 2001). Significantly less attention has been given to hydrophobic magnetic elastomers, which include a few instances of polydimethylsiloxane (Evans et al., 2007; Fahrni, Prins, & van Ijzendoorn, 2009; Jolly, Carlson, Munoz, & Bullions, 1996; Varga, Feher, Filipcsei, & Zrinyi, 2003) and polystyrene (Timonen et al., 2010).

A material which is to be useful in the fabrication of a microactuator must be chemically and osmotically compatible with its target environment, contain a large volume fraction of magnetic nanoparticles, and have a low modulus. Since the target environment for most biological and biomimetic applications is aqueous, a hydrophobic matrix is helpful in meeting the first requirement. A hydrophobic magnetic elastomer resists swelling in an aqueous environment, and nanoparticles effectively encapsulated in the hydrophobic matrix are unlikely to leech into an aqueous environment. The lack of swelling, however, generally

gives hydrophobic elastomers a significantly higher modulus than their hydrophilic peers, which are usually fabricated in a swollen state and are able to remain so due to the presence of water as a good solvent.

We will therefore explore two different materials as candidates for magnetic microactuators. The first is a hydrogel consisting of maghemite (Fe_2O_3) nanoparticles in a polyacrylamide matrix, and the second is a complex of maghemite nanoparticles in a hydrophobic siloxane matrix.

2.4 Hydrogel-based composites

Hydrogels are, by definition, any polymeric material which is swollen to a great degree, generally greater than 90%, with water (Mathur, Moorjani, & Scranton, 1996). They may be crosslinked, such as in an acrylamide gel or most polyvinyl alcohol hydrogels, or uncrosslinked, as in agarose. Although hydrogels are susceptible to osmotic effects while in an aqueous environment and are therefore likely to well or shrink unpredictably, they offer several advantages over silicone elastomers which make them attractive. Most intriguing is their affinity for water, which gives them an extremely low surface energy in an aqueous medium. This property has the potential to reduce the incidence of collapse due to self-adhesion which is prevalent in high-aspect-ratio hydrophobic structures (Evans et al., 2007; Roca-Cusachs et al., 2005). In addition, aqueous ferrofluids mix readily into many hydrogels, simplifying synthesis and allowing for relatively high concentrations of magnetic material. Finally, most hydrogels have very low elastic moduli (1-100 kPa), resulting in very flexible structures, and in many cases the modulus may be tuned simply by adjusting the ratio of polymer to water.

Incorporating nanoparticles into a hydrogel results in a magnetic elastomer. In the case of a hydrogel, the magnetic nanoparticles can either be precipitated directly within a crosslinked matrix (H. Lin et al., 2003) or the polymer and particles may be synthesized separately and mixed together prior to crosslinking (Galicia et al., 2003; Mayer et al., 2000; Szabo et al., 2000).

A prime candidate for a hydrogel-based magnetic elastomer is a maghemite-impregnated polyacrylamide. In the fabrication of a polyacrylamide magnetic elastomer, a citrate-stabilized pH 7 maghemite nanoparticle ferrofluid can be mixed directly into an aqueous solution of acrylamide monomer. The low viscosity and absence of long-chain polymers at this stage allows the ferrofluid to mix well even at very high concentrations, after which polymerization and crosslinking are performed simultaneously, forming a gel in which the maghemite particles are trapped. In this manner, materials have been produced with maghemite concentrations as high as 18% v. (50% wt.) and with elastic moduli as low as 10^4 Pa (Galicia et al., 2003; Mayer et al., 2000). So stable is the ferrofluid that we have found that the upper limit on concentration results from a mechanical limitation – the fluid becomes to pasty to be workable much above 18% v., yet shows no sign of flocculation.

Following Galicia et al., a typical recipe for an acrylamide magnetic elastomer requires the acrylamide monomer (AM), a bisacrylamide crosslinker (N, N methylene bisacrylamide, or BA), catalyst (ammonium persulfate, APS) and an initiator (tetramethylethylenediamine, TEMED). Polymerization and crosslinking necessarily occur simultaneously, as the symmetric bisacrylamide forms crosslinks by becoming incorporated in adjacent polymer chains during polymerization. Synthesis of a representative sample of a ferrofluid-acrylamide material (FFAAm) which contains 6% wt. acrylamide in water would proceed as follows:

The monomer (AM) and crosslinker (BA) are mixed in a ratio of 20 to 1 in a 20% wt. solution in deionized water (2.22 grams AM and 0.11 grams of BA into 10 mL H_2O). This solution is

diluted with a citrate-stabilized ferrofluid of a given maghemite concentration to produce a ferrofluid-acrylamide solution of 6% wt. polymer (0.54 mL AM/BA mixture to 1.46 mL citrate-stabilized ferrofluid). Since oxygen is known to interfere with the free-radical decomposition products of the APS, the solution is degassed with argon for 10 minutes prior to crosslinking and the subsequent reaction is performed in a nitrogen environment. Crosslinking occurs upon the addition of 0.2% wt. APS (40 uL of 10% APS in H_2O) and 0.2% TEMED, and is complete within a couple of minutes.

2.5 Silicone-based composites

Only a few instances of hydrophobic magnetic elastomers occur in the literature. These materials, however, have several advantages over their hydrophilic cousins when implemented in an aqueous environment: they are unlikely to interact chemically or osmotically with the environment and are less likely to leech nanoparticles. The scarcity of hydrophobic magnetic elastomers relative to their hydrophilic peers is likely the result of the additional complication of treating iron oxide nanoparticles to make them miscible in a non-polar matrix. (In-situ precipitation of nanoparticles within a crosslinked matrix has not been explored in this case, since current techniques precipitate nanoparticles in an aqueous solution.)

While larger particles (> 1 micron) can be mixed directly into a siloxane polymer by brute force, this results in a material that is heterogeneous at the microscale and therefore likely unsuitable for application in magnetic microactuators. To achieve homogeneity at the micron scale, great care must be taken to ensure the colloidal stability of the nanoparticles. Such stability may be achieved through the use of surfactants (Evans et al., 2007) or by strong adsorption of a hydrophobic chemical species on the surface of the particle (Mefford et al., 2008; Rutnakornpituk et al., 2002; Stevenson et al., 2001; Wilson, Goff, Riffle, Harris, & St Pierre, 2005). A description of the preparation of the former follows.

Magnetite nanoparticles are first prepared via the coprecipitation of iron salts (Massart, 1981) and are further oxidized to form maghemite by heating in an acidic solution in the presence of iron nitrate. The particles are then grafted with oleic acid (van Ewijk et al., 1999). The presence of oleic acid serves to enhance the solubility of the nanoparticles in a non-polar solution; however, mixing directly with a silicone elastomer such as Dow Corning Sylgard 184 results in flocculation of the nanoparticles and further action is required to achieve a homogenous solution. Before mixing, hexadecane is added in a 1:1 v/v ratio with the oleic acid nanoparticle suspension and the entire product is diluted 5:1 in toluene. Sylgard 184 prepolymer is similarly diluted in toluene, and the two solutions are combined over the course of several minutes under the influence of immersion ultrasonication. The toluene is then removed by evaporation. After resting for several days, excess hexadecane and Sylgard 184 will separate from the composite. Decantation yields a stable suspension of maghemite nanoparticles in a poly(dimethyl siloxane) matrix. This material is produced without any curing agent in order to extend its shelf life.

3. Fabrication

3.1 Template candidates

The two primary strategies that have emerged for fabricating magnetic cila are self-assembly and template-based methodologies. In the first, an applied magnetic field is used to cause the material to assemble into an energetically-favorable arrangement. Minimization of magnetic

energy at the expense of surface energy can lead to elongated structures which are suitable for magnetic actuation applications. These self-assembled structures may consist of either an uncrosslinked magnetic polymer composite (Timonen et al., 2010) or a series of magnetic beads (Furst, Suzuki, Fermigier, & Gast, 1998; Singh, Laibinis, & Hatton, 2005; Vilfan et al., 2010), which may or may not be crosslinked prior to the removal of the external field.

The most common template-based fabrication strategy is soft lithography, in which soft polymeric structures are templated in a photolithographic mold, which is generally constructed of photoresist on a silicon substrate. However, while soft lithography is capable of producing structures of very high aspect ratio in a plane parallel to the surface (length >> width), it is not well-suited to producing high-aspect ratio structures in a plane perpendicular to the surface (depth >> width). This limitation may be attributed to photon scattering during the exposure of the resist. Furthermore, with soft materials such as silicones and hydrogels, photolithographic lift-off procedures may lead to structure collapse (Pokroy, Epstein, Persson-Gulda, & Aizenberg, 2009; Roca-Cusachs et al., 2005; Zhang, Lo, Taylor, & Yang, 2006).

Another common template for high-aspect-ratio microstructures is anodized aluminum oxide (AAO) (Chik & Xu, 2004; McGary et al., 2006). AAO offers the advantage of a gentle removal of the template by dissolution and may be grown to a wide range of thicknesses, enabling the production of microstructures of various length. However, AAO imposes severe limits on both the diameter and the spacing of the microstructures, which may limit its application.

Track-etched membranes have also been used in the synthesis of nanostructures (Huczko, 2000; Hulteen & Martin, 1997) – most notably metallic nanowires (Brumlik, Menon, & Martin, 1994; Schonenberger et al., 1997) – and they present a third possibility for a template for the production of biomimetic cilia. These membranes generally consist of a very thin layer of polymer (most commonly polycarbonate) which is exposed to high-energy ions from a nuclear source or ion beam. As the ions travel through the polymer, they leave behind a track of broken bonds (about 10 nm diameter) surrounded by a halo of additional damage (10 – 100 nm) (Fischer & Spohr, 1983). The particle tracks etch preferentially in a solution of sodium hydroxide to produce pores of a uniform and tunable diameter (Ferain & Legras, 1997; Fischer & Spohr, 1983). Polycarbonate track etched (PCTE) membranes are available in a variety of thicknesses and pore densities, allowing for the production of microstructures in a variety of lengths and inter-structure spacing. They are also soluble in organic solvents such as dichloromethane (DCM) and N-methylpyrrolidone (NMP), among others, allowing for the gentle removal of the membrane from the molded structures.

3.2 Sample design considerations

In its simplest manifestation, template-based fabrication of biomimetic cilia from one of the aforementioned materials would require filling the template with material, crosslinking the material, and then removing the membrane by dissolution. There are, however, several considerations which impose further requirements. For example, micro- and nanostructured materials are highly susceptible to collapse during drying due to surface tension forces. While such damage may be alleviated by the use of a critical point dryer, it is most convenient to process the samples in such a way that they remain submerged. We will present a fabrication method below which maintains a fluid environment at all times.

In addition, completed cilia arrays will be actuated by a magnetic source which should be as close as possible to the cilia array to allow for the largest possible applied fields. Cilia arrays

should also be fabricated in such a way as to facilitate high-magnification optical microscopy. Fig. 2I presents a configuration which allows for both high-magnification optical microscopy and optimal placement of a magnetic source. In this configuration, the magnetic source is placed directly above the sample. This would block the light path in conventional transmission microscopy; however, a reflective gold-coated cover slip placed just above the sample allows for imaging in reflection. It should be noted that this is not traditional reflection microscopy as the incident light does not reflect directly off the sample itself, but is transmitted through the sample after reflecting from the gold coating. This configuration places an additional constraint on the sample configuration: in order to be close to both the magnetic source and the objective, the sample should be made as thin as possible.

We will present a fabrication method below which can be used to produce samples as thin as 500 microns. In this example, we will assume that the cilia are fabricated of a silicone-based magnetic elastomers templated in a polycarbonate track-etched membrane. Modifications are necessary, of course, for hydrogel-based magnetic elastomers such as acrylamide (see section 3.4), but the bulk of the processing remains the same.

3.3 Fabrication of silicone-based microstructures

Before beginning a discussion of the fabrication procedure, we should note that one critical element in the following is the adhesion of the silicone cilia to a glass substrate. Generally, silicone exhibits an affinity for glass – even when submerged in water, silicone cured in contact with a glass cover slip will readily adhere to the glass surface. However, an organic solvent such as that used to dissolve a template will quickly swell the silicone and cause it to release from the glass surface. In addition, the same solvent will often render epoxies and other adhesives useless. It is best then to secure the silicone directly to a firm glass substrate via a covalent bond. This may be done by oxidizing the surfaces of both the glass and the silicone with an oxygen plasma, ultraviolet light, or corona discharge (Berdichevsky, Khandurina, Guttman, & Lo, 2004; Efimenko et al., 2005; Efimenko, Wallace, & Genzer, 2002; Makamba, Kim, Lim, Park, & Hahn, 2003), after which the surfaces will bond on contact via a condensation reaction.

A typical fabrication procedure for silicone-based biomimetic cilia would then proceed as follows. A polycarbonate track-etched (PCTE) membrane is selected with an appropriate thickness and pore density, and is etched in a sodium hydroxide solution to achieve the appropriate pore diameter. We find that a solution of 4 M NaOH heated to 80° C will preferentially etch the pores of a PCTE membrane to increase pore diameter at a rate of about 15 nm/min. After etching, the membrane is impregnated with liquid magnetic elastomer, and the surface of the membrane is cleaned thoroughly with a lab wipe moistened with ethanol (Fig. 2A).

A cover slip is prepared to receive the membrane by affixing a thin rectangular ring of silicone elastomer via the oxidation/condensation reaction described above. This ring will act as a spacer between the upper and lower cover slips in the final product, and should be sized accordingly. The impregnated membrane is then submerged in a small amount of uncured silicone elastomer containing curing agent and placed within the silicone ring (Fig. 2B). Care should be taken to ensure that the uncured silicone is in good contact with the silicone well – it is the well which is chemically bound to the glass; the encapsulating silicone is bound only to this well. The sample is then cured by heating to 80° C for one hour. While the silicone–nanoparticle composite described in Section 2.5 will contain no
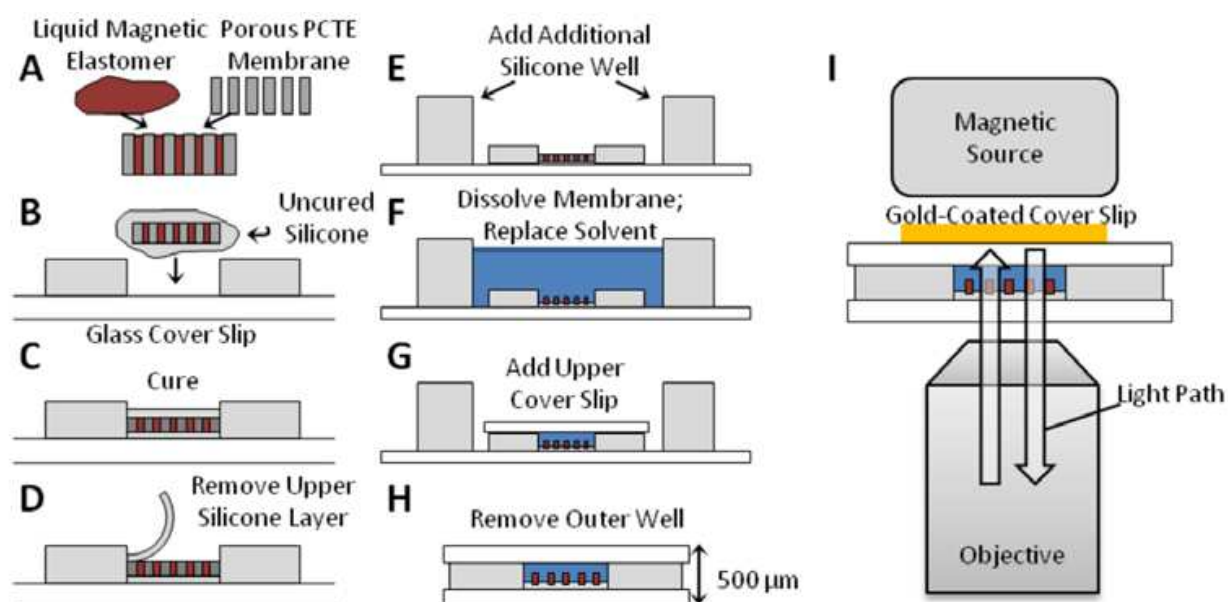
Fig. 2. A-F: Fabrication of silicone-based magnetic biomimetic cilia. I: Modified optical reflection microscopy for viewing biomimetic cilia under magnetic actuation.

curing agent, we have found that the curing agent contained in the surrounding silicone diffuses sufficiently into the composite material, resulting in reliable crosslinking. Finally, the sample is prepared for dissolution by exposing the upper face of the membrane via the removal of the upper layer of cured, encapsulating silicone (Fig. 2D). This layer may be cut carefully with a scalpel and peeled away.

The sample is quite robust only until the membrane is dissolved, and so after dissolution the exposed cilia should remain continually submerged in a liquid. The thin silicon spacer is not enough to reliably retain a liquid bath around the cilia, and so a larger temporary well is added just outside the small well (Fig. 2E). This well must be affixed via the oxidation/condensation reaction previously described to avoid release during dissolution, but will be removed with a razor blade later.

The membrane is then dissolved by submerging the entire sample in a bath of solvent, such as dichloromethane. We have found that heating the solvent results in quicker dissolution and a greater number of viable cilia in the final product, so it is advantageous to heat the solvent to just below its boiling point (about 40° for dichloromethane) before dissolving the membrane. Since dichloromethane is immiscible with water, it is advisable to replace the solvent first with ethanol, after which it may be transferred to water.

Finally, a piece of cover slip is cut to fit within the outer well and is placed on top of the inner well, as shown in Fig. 2G. Excess fluid is removed, and the outer well can be carefully cut free with a razor. This upper cover slip is not permanently attached, but evaporative effects will produce a small vacuum and fix the cover slip in place quite well. For longer term storage, the entire sample may be submerged in a fluid bath. The completed sample can be designed to be less than 500 microns thick; this dimension is limited mostly by the dimensions of the upper and lower cover slips.

3.4 Process modifications for hydrogels

The fabrication procedure for hydrogel-based biomimetic cilia is very similar, but requires a few modifications. The most significant of these is the manner in which the polymer is
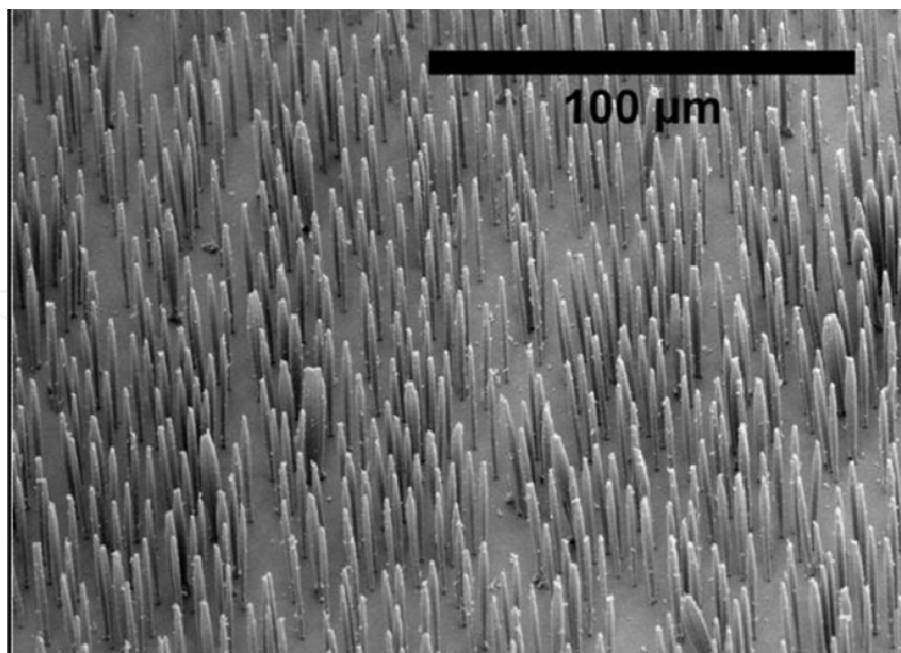
Fig. 3. Biomimetic cilia fabricated of a maghemite-nanoparticle / polydimethyl-siloxane composite by the techniques described in this section.

affixed to the glass substrate. The oxidation/condensation reaction that worked for the silicone materials is useless here, and it can be a challenge to find a suitable substitute. Sidorenko et al. have developed a method of bonding an acrylamide hydrogel to glass by first oxidizing the glass by plasma, corona, or UVO treatment and then using the available hydroxyl groups to bond poly(glycidyl methacrylate) (PGMA) to the surface. The epoxy groups of the PGMA are then functionalized with acrylic acid, which will become incorporated within in the polyacrylamide backbone upon polymerization, permanently bonding the polymer to the glass (Sidorenko, Krupenkin, Taylor, Fratzl, & Aizenberg, 2007). In addition, prepolymers of hydrogel-based magnetic elastomers generally have a much lower viscosity than silicon-based elastomers, and so it is uncertain whether the uncured magnetic elastomer material would remain within the pores of the PCTE membrane upon submerging the sample in the encapsulating hydrogel layer (as in Fig. 2B). For this reason, the membrane is submerged in a bath of magnetic elastomer and the entire bath is cured; the membrane is then removed and cleaned before submersion in the encapsulating hydrogel layer.

4. Actuator design

4.1 Introduction

Since the advent of viable experimental models of cilia-like magnetic structures (Evans et al., 2007; Furst et al., 1998), a number of works have been presented which propose detailed computational models describing their actuation (Alexeev, Yeomans, & Balazs, 2008; Downton & Stark, 2009; Evans et al., 2007; Gauger, Downton, & Stark, 2009; Shcherbakov & Winklhofer, 2004). In addition, a few authors have published on the energy of rotating magnetic droplet (Cebers, 2002; Morozov, Engel, & Lebedev, 2002). While many of these models take into account dynamics such as fluid-structure interactions and polymer viscosity, we will confine ourselves here to a quasi-static model. Such a model is

independent of the application of biomimetic cilia structures and is more than suitable for providing a set of guidelines for the design of magnetic cilia.

4.2 Actuation in a uniform field
4.2.1 A simple model
We will assume the cilium is cantilevered perpendicular to the substrate, and the elastic energy therefore increases with displacement from the vertical (Fig. 4). Since magnetic elastomers are generally superparamagnetic and therefore have no remanence magnetization, any magnetic torque is the result of shape anisotropy. The shape anisotropy of a high-aspect-ratio cilium results in a demagnetizing field along its short axes, which affects both the direction and magnitude of the resulting magnetization. Specifically, the magnetic energy is minimized when the magnetization of the cilium lies along its long axis and this results in a torque which causes it to tend to align with an applied field.

Thus, we can write down the energy of a magnetic cilium as the sum of elastic and magnetic energies:

$$U = \frac{1}{2}EI\int_0^L \frac{1}{R(s)^2}ds - \frac{\mu_0 V}{2}\left[G^2 M'\left(\frac{\cos^2\theta}{H+N_x M'} + \frac{\sin^2\theta}{H+N_y M'}\right) - M'H + 2\int_0^H M'(H')dH'\right] \quad (1)$$

where G and H are related by

$$\frac{1}{G^2} = \frac{\cos^2\theta}{H+N_x M'(H)} + \frac{\sin^2\theta}{H+N_y M'(H)} \quad (2)$$

Here, the elastic energy is described by the Kirchhoff model (Landau & Lifshitz, 1986) of a uniform elastic rod, where E is the Young's modulus of the cilium, I is the bending moment, and R is the radius of curvature of the cilium which is in general a function of s, the distance along the contour of the cilium from its base. In the magnetic energy term (Morozov et al., 2002), G is the applied magnetic field (in A/m), M' is the magnetization of the cilium, which in general is a function of H, the internal field (in A/m). The angle between the cilium and the applied field is given by θ, and N_x and N_y are the demagnetization factors parallel and perpendicular to the axis of the cilium, respectively. V is the volume of the cilium.

We have found that the magnetization of a magnetite-polymer composite is linear with respect to the volume fraction of magnetic particles even to very high loadings (90% wt.). Therefore to make explicit the effect of nanoparticle loading, we will henceforth write the magnetization of the composite material, M', in terms of the magnetization of the magnetic component, M, and the volume fraction of magnetic nanoparticles, f, or $M' = Mf$.

Much of the complexity in equations (1) and (2) stems from the fact that shape anisotropy affects both the direction *and* magnitude of the magnetization, M. However, the influence of anisotropy on the total energy due to its effect on the magnitude of M is secondary to its effect on direction. If we therefore consider a simplification in which the magnitude of the magnetization is dependent only on the internal field, H and not on the orientation of the cilium, then we can describe the magnetic energy with the Stoner-Wohlfarth model (Stoner, 1947), in which case the total energy becomes:

$$U = \frac{1}{2}EI\int_0^L \frac{1}{R(s)^2}ds - \frac{1}{2}\mu_0 M^2 f^2 V\left(N_x - N_y\right)\cos^2\theta \quad (3)$$

These two models converge for saturating fields, and in the case of small fields the Stoner-Wohlfarth model will underestimate the calculated applied field magnitude by a factor of $\sqrt{1 + \chi N_x}$, where $\chi = M/H$ is the dimensionless magnetic susceptibility. This factor is greatest for highly permeable materials and very small fields. In the extreme limit of a material which consists of 100% iron oxide and for fields approaching 0 T, we find that the resulting error is approximately a factor of 2; in most cases the error is less than 10%. This is more than sufficient accuracy for an investigation of design considerations of magnetic cilia, and this simplification will enable us to derive several useful expressions to guide design considerations.
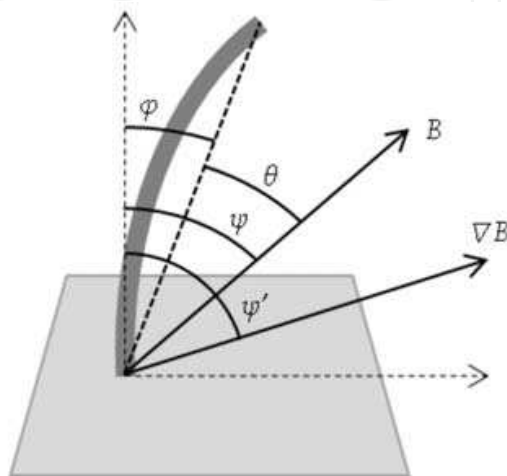

Fig. 4. Angle definitions used in the model. An upright elastic cilium which is cantilevered from a horizontal surface bends through an angle of φ due to the presence of a magnetic field, B, and/or a magnetic field gradient, $\nabla \boldsymbol{B}$.

4.2.2 Field requirements

We would like to consider the necessary requirements for successful actuation of a magnetic cilia. Let us therefore define the lower limit of 'successful' action as a 10° bend from the vertical, where the angle is defined to be between a line connecting the base of the cilium to the tip and the vertical (Fig. 4). In the case of a 10° bend, it is reasonable to approximate the radius of curvature of the cilium as constant along the length, in which case we can allow $R = L/2\varphi$ in Equation (3). In addition, in the limit of high aspect ratio ($L/2r > 20$), the difference between the demagnetization factors N_x and N_y approaches ½. Since a typical epithelial cilium has an aspect ratio of about 35, we will henceforth assume that this is the case. Taking a derivative to find the torque on the cilia, we see

$$\tau = \pi \frac{Er^4}{L}\varphi - \frac{1}{2}\mu_0 M^2 f^2 V \cos(\psi - \varphi)\sin(\psi - \varphi) \qquad (4)$$

where we have used $\theta = \psi - \varphi$ to make the angular dependencies more explicit (Fig. 4). One interesting thing to note in this expression is that the magnetic torque on the cilium is always maximized when $\theta = 45°$. Let us assume that the field is applied in this optimal orientation; then the magnetization required to achieve a bending of φ is given by the simple expression:

$$M = \frac{1}{f}\sqrt{\frac{E}{\mu_0}}\frac{2r}{L}\varphi^{1/2} \tag{5}$$

The applied field can be mapped to magnetization via the full magnetization curve of the chosen nanoparticle. In Fig. 5, we show the magnetic field required to bend a cilium of radius 100 nm and length 10 microns (typical of epithelial cilia) through an angle of 10°.
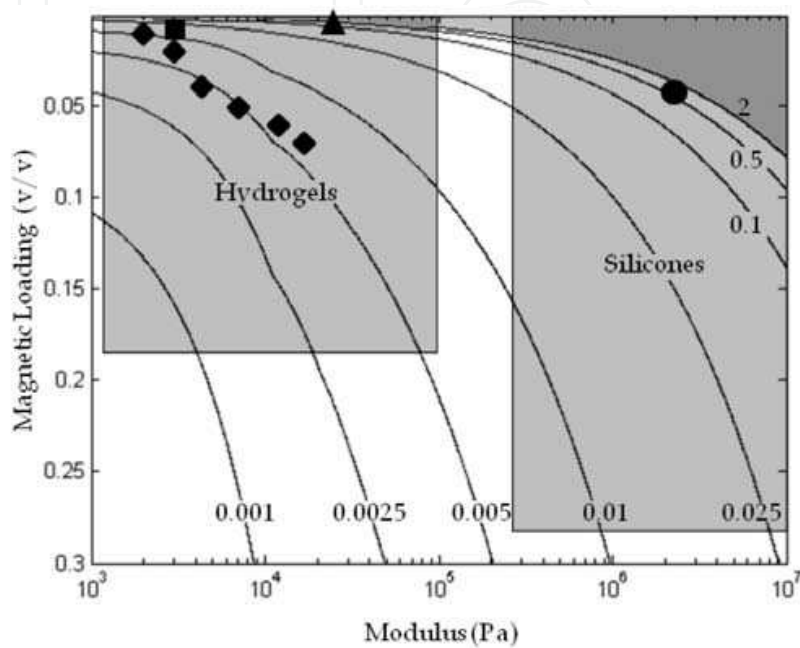

Fig. 5. The magnetic field in tesla (T) required to bend a 7-micron tall magnetic cilium of 100 nm radius through an angle of 10°. The cilium is loaded with maghemite nanoparticles. Superimposed on the plot are instances of reported magnetoelastomers. Diamonds: maghemite/polyacrylamide (Galicia et al., 2003); Square: magnetite/polyvinyl alcohol (Barsi et al., 1996); Triangle: M-300/polyvinyl alcohol (Collin et al., 2003); Circle: maghemite/poly(dimethyl siloxane) (Evans et al., 2007).

In Fig. 5, we have highlighted the regions of the parameter space which are feasibly accessible with current materials. The glyphs indicate reported magnetic elastomers, which also appear in Table 1. The shaded areas indicate the range of moduli of common hydrogel and silicon elastomers independently of whether they have been employed in a magnetic nanoparticle composites, and the range of magnetic nanoparticle loading in hydrogel and silicone composites independently of whether the composite has been crosslinked. Most notable in the latter group is a poly(dimethyl siloxane) – magnetite composite fluid which contains nanoparticle loadings up to 28% v/v (Wilson et al., 2005). Similarly, polyacrylamide hydrogels with maghemite loading up to 18% have been described (Mayer et al., 2000), but moduli have not been reported for these materials.

It is interesting to note that in the region above 2 T in the extreme upper-right of the plot represents an area of the parameter space in which it is impossible to bend a cilium through the required angle with *any* field magnitude. This occurs because the applied field has fully saturated the cilium at this point, and further contributions have no effect. This saturation effect is not an artifact of our simplified model; though not quite so explicit, the limitation also exists in Equation (1).

4.2.3 Material design

We have thus far described the magnetic field required to actuate a cilium of known composition and aspect ratio. However, from the point of view of materials design, it would be useful to have a figure of merit which indicates how well suited a material is for magnetic actuation applications, regardless of geometry. Such a figure could be used to optimize a material with respect to tunable parameters such as modulus and magnetic content. In the case of an optimally-applied field, we can solve Equation (5) for the bend angle φ, in which case

$$\varphi = \frac{\mu_0 M^2 f^2}{E}\left(\frac{L}{2r}\right)^2 \tag{6}$$

The second part of this expression is the square of the aspect ratio, and contains all of the geometrical parameters of the cilium. The first contains only material properties, and is therefore useful in designing materials for use in magnetic actuation devices. In this work, therefore, we refer to the first term as the magnetoelastic ratio. It is important to note that the dependencies on magnetization M and Young's modulus E are not necessarily independent, since adding magnetic content to the composite material generally results in an increase in modulus. Measurements of the modulus of a particular material as a function of particle loading can therefore be used to determine an optimal loading for maximal actuation.

			Magnetoelastic Ratio	
	f	E (kPa)	Field Bending	Gradient Bending
Maghemite/Polyacrylamide*	0.01 – 0.07	2-16	0.0650	1.680
Magnetite / Poly(vinyl alcohol) †	0.009	3	0.0078	0.072
M-300 / Poly(vinyl alcohol) ‡	0.005	25**	0.0003	0.048
Maghemite / Poly(dimethyl siloxane) §	0.04	2500	0.0002	0.003

Table 1. Magnetoelastic ratios for reported magnetic elastomers with nanoscale magnetic particles, for both field-dominated bending and gradient-dominated bending. *(Galicia et al., 2003); †(Barsi et al., 1996); ‡(Collin et al., 2003); §(Evans et al., 2007); **estimated from reported shear modulus.

The preceding table details the magnetoelastic ratios of extant composite materials for which both nanoparticle concentration and modulus were reported (Table 1). Magnetoelastic ratios as a function of particle loading for the first material on this table are shown in Fig. 7.

4.3 Actuation by a field gradient
4.3.1 Modeling

We have thus far only considered the case of a constant magnetic field, in which the mechanism for actuation is the tendency for the long axis of the microactuator to align with the applied magnetic field due to shape anisotropy. However, another mode of actuation exists in the presence of a magnetic field gradient. Any paramagnetic material – regardless of geometry – will be attracted toward regions of higher field, i.e. along a magnetic field gradient. We can account for this type of bending in our energy model simply by adding a term for the energy of a magnetic moment in a magnetic field: $U = -mB\cos\alpha$, where α is the angle between the magnetic moment and the applied field. It can be shown that for the vast majority of magnetic nanoparticle composite materials, $\alpha \sim 0°$; that is, the magnetic moment

aligns with the applied field rather than with the easy axis of the rod (Evans et al., 2007). Thus, energy is minimized when an actuator bends toward a region of higher magnetic field, B.

To first order, we will assume that m is constant with respect to a bend through an angle φ, and that the magnetic field B has a constant gradient. Then upon integrating this energy over length of the rod, we find that the total energy is given by

$$U = \frac{1}{2}EI\int_0^L \frac{1}{R(s)^2}ds - \frac{1}{2}\mu_0 M^2 f^2 V\left(N_x - N_y\right)\cos^2(\psi - \varphi) - \frac{1}{2}MfV\nabla BL\cos\left(\psi' - \varphi\right) \tag{7}$$

where the final term represents the contribution of the magnetic field gradient. In this term, ψ' is the angle of the magnetic field gradient relative to the vertical (Fig. 4), and for consistency we have replaced the magnetic moment m with the magnetic moment per unit volume M multiplied by the volume of the actuator, V.

4.3.2 Gradient requirements

The net torque on the microactuator is then

$$\tau = \pi\frac{Er^4}{L}\varphi - \frac{1}{2}\mu_0 M^2 f^2 V\cos(\psi - \varphi)\sin(\psi - \varphi) - \frac{1}{2}MfV\nabla BL\sin(\psi' - \varphi) \tag{8}$$

where we have again assumed constant curvature and high aspect ratio.

Bending within the field-dominated regime is described earlier in this document. In the case of gradient-dominated bending, we can turn off the magnetic field torque term in Equation (8) simply by requiring that the magnetic field direction align at all times with the axis of the actuator ($\psi = \varphi$). Solving for the condition of zero net torque, we find that the magnetic field gradient necessary to bend an actuator through an angle φ in a gradient-dominated regime is given by

$$\nabla B = \frac{2E}{Mf}\frac{r^2}{L^3}\varphi \tag{9}$$

In Fig. 6 we show the magnetic field gradient, in T/m, required to bend a cilium of radius 100 nm and length 7 microns (typical of epithelial cilia) through an angle of 10°.

4.3.3 Materials design

Furthermore, in the case of gradient-dominated bending we can develop a term analogous to the magnetoelastic ratio for field bending introduced in Section 4.2.3. To do so, we rewrite Equation (9) to solve for the bend angle φ:

$$\phi = \frac{Mf}{2E}\frac{L^3}{r^2}\nabla B \tag{10}$$

The first term of this expression contains all of the material properties of the microactuator and is independent of geometrical considerations. As such, it serves as a figure of merit for the suitability of material for application in gradient-dominated magnetic microactuation applications. Magnetoelastic ratios of extant composite materials for gradient bending are reported in Table 1.
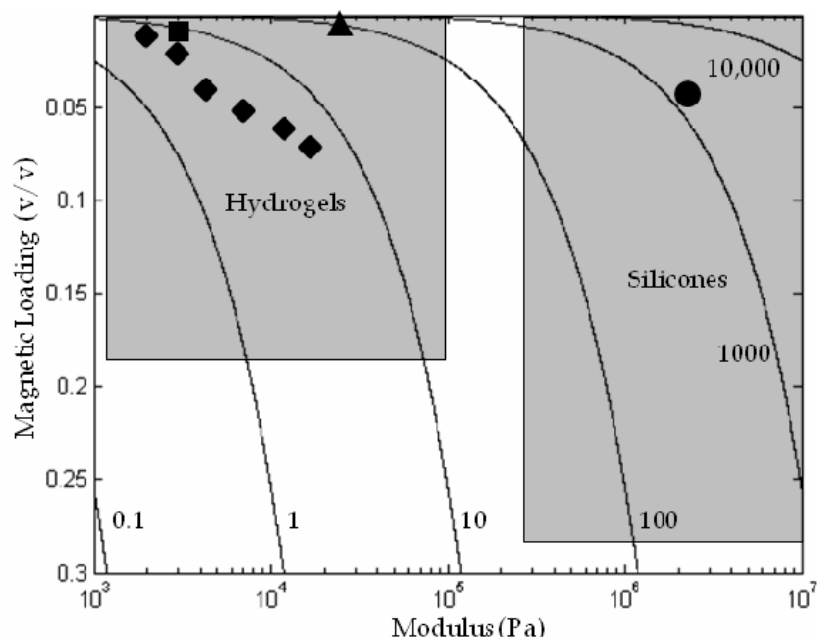
Fig. 6. The magnetic field gradient in tesla per meter (T/m) required to bend a 7-micron tall magnetic cilium of 100 nm radius through an angle of 10°. The cilium is loaded with maghemite nanoparticles, and is assumed to be magnetically saturated. Superimposed on the plot are instances of reported magnetoelastomers. Diamonds: maghemite / polyacrylamide (Galicia et al., 2003); Square: magnetite / polyvinyl alcohol (Barsi et al., 1996); Triangle: M-300 / polyvinyl alcohol (Collin et al., 2003); Circle: maghemite / poly(dimethyl siloxane) (Evans et al., 2007).

In Fig. 7, below, we plot the magnetoelastic ratios for both field bending and gradient bending for a maghemite / polyacrylamide magnetic elastomer reported by Galicia et al. Both curves show a clear optimization at a 4% nanoparticle loading; at higher nanoparticle concentrations, the increase in modulus due to the nanoparticle component outweighs the additional magnetization. Similarly, it is clear in Fig. 5 and Fig. 6 that the f = 0.04 sample of this material is predicted to bend at the lowest values of magnetic field and field gradient, respectively.

5. Actuation strategies

5.1 Introduction
The biomimetic cilia in this discussion are designed to be actuated magnetically, and there are three possible means for producing a magnetic field: with a current-carrying wire, with a permanent magnet, and with an electromagnet. A current-carrying wire holds a certain amount of appeal, since such would provide a great degree of flexibility in producing a time-varying magnetic field. One can imagine an array of lithographed wires supplanted beneath the cilia array which might be individually addressed to produce a synchrony of temporally and spatially manipulated magnetic fields. While such an image is enticing, no one has yet achieved actuation of magnetic cilia with a current-carrying wire, although possibilities have been discussed in the literature (Fahrni, Prins, & van IJzendoorn, 2009). We will discuss difficulties and possibilities for this sort of actuation below.

Permanent magnets, on the other hand, have been successfully used to actuate magnetic cilia arrays (Evans et al., 2007), and are attractive due to their relatively large fields and ease
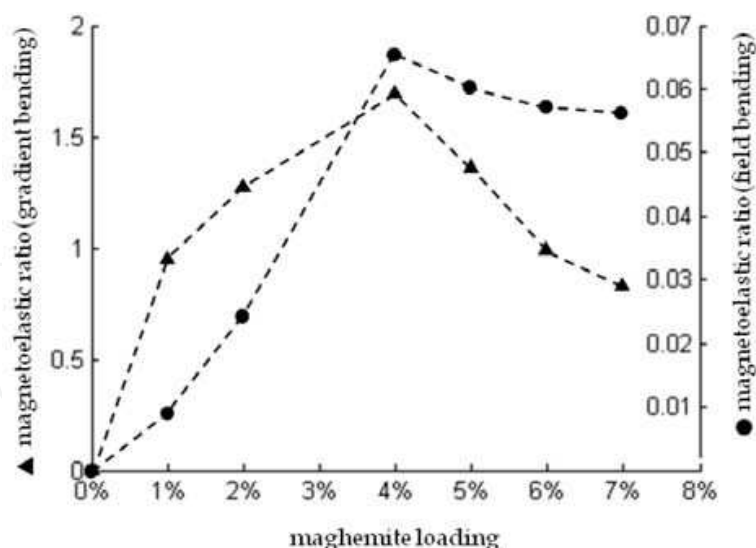
Fig. 7. Magnetoelastic ratios as a function of maghemite nanoparticle loading for a maghemite / polyacrylamide magnetic elastomer reported by (Galicia et al., 2003).

of implementation. A detailed discussion of actuation via permanent magnet will follow. Finally, electromagnets may be considered an extension of the prior two methods, combining the flexibility of the current-carrying wire with the strength of a permanent magnet. Excepting the case of superconductors, however, macroscopic wires or electromagnets can at best approach the field magnitudes generated by permanent magnets and will therefore not be considered in-depth in this work. To date no one has reported actuation with an electromagnet or electromagnet array, although such might be possible with an extant micromagnetic apparatus such as the 3DFM (Fisher et al., 2006).

5.2 Field or gradient dominance

Before we begin a discussion of these mechanisms, however, we first recognize that bending may occur in two distinct regimes – field-dominated or gradient-dominated – as previously described. To better understand the magnetic field geometries characteristic of each, we take the ratio of 'gradient' torque to 'field' torque, and find that

$$R = \frac{2\nabla BL}{M(B)\mu_0 f} \tag{11}$$

Here we have written the magnetization as function of magnetic field in order to make the role of the magnetic field magnitude explicit. Fig. 8 displays in the parameter space of applied field and field gradient contours on which the ratio R is unity. Here we have selected a length L of 7 microns and maghemite as the loading material. We have chosen three representative values of particle loading f, which cover the gamut of extant materials. The region to the upper-left of each $R=1$ contour is field-dominated; the region to the lower-right of each is gradient-dominated.

5.3 Permanent magnets

Perhaps the most straight-forward way to actuate a magnetic microstructure is by introducing a permanent magnet. Currently, rare earth magnets such as those constructed of neodymium-iron-boride (NIB) offer the largest fields of available magnets. With internal
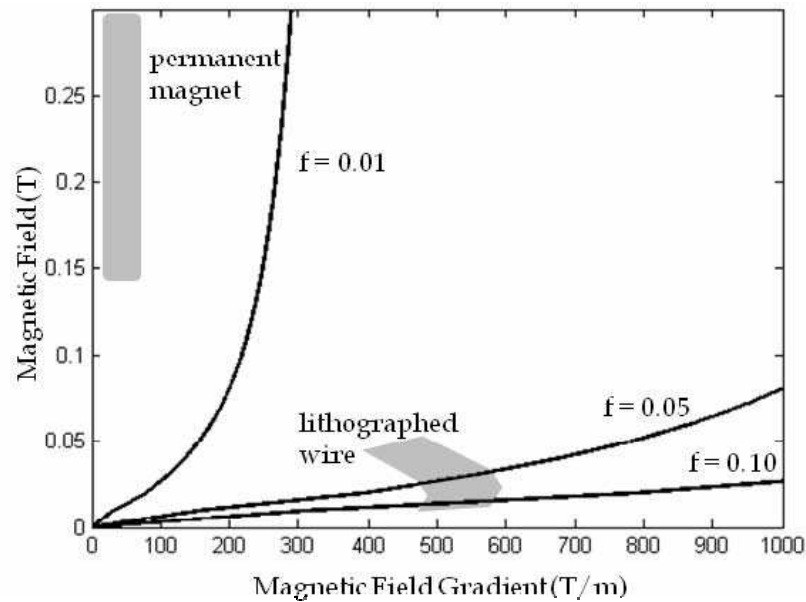
Fig. 8. Field-vs.-Gradient dominance for a cilium of length 7 microns. Lines represent R = 1 contours, on which the torque due to the magentic field and torque due to the magnetic field gradient are equal. R = 1 lines are shown for different values of maghemite nanoparticle loading, *f*. Regions to the upper-left of each of these lines is field-dominated; regions to the lower-right are gradient-dominated. Shaded regions indicate regions of the parameter space accessible by permanent magnets and lithographed wires.

fields of approximately one tesla, the magnetic field available at the surface of such magnets is approximately 0.5 tesla. This is largely independent of the size of the magnet itself; however, the size of the magnet does determine how quickly the field decays with distance from the magnet – i.e. the gradient. From our own measurements, we find that the field strength at a reasonable working distance of 3-mm from various sizes of NIB magnets ranges from about 0.15 – 0.25 tesla, and the magnetic field gradients at similar distances ranges from 30 – 60 T/m. Measurements were taken on 6-mm-thick cylindrical magnets with radii ranging from 25 - 50 mm. This region is highlighted in Fig. 8; it is clear from this plot that magnetic actuation of biomimetic cilia with permanent magnets will generally be field-dominated. However, in certain circumstances the magnetic field gradient from a permanent magnet can be locally enhanced by affixing a sharp pole tip (Evans et al., 2007).

5.4 Current-carrying wires
The magnetic field and field gradient generated by a current-carrying wire is given by

$$|B| = \frac{\mu_0 I}{2\pi r}; \quad |\nabla B| = \frac{\mu_0 I}{2\pi r^2} \tag{12}$$

where I is the current through the wire and r is the distance from its center. For the case of a single, macroscopic wire, both the field and field gradient generated are negligible in the context of magnetic actuation of biomimetic cilia. Constructions of multiple wires such as solenoids or Helmholtz coils certainly generate significantly larger magnetic fields; however these fields are similar in geometry and yet far weaker than those produced by permanent magnets, and will not be considered here.

In the realm of the microscopic, however, one might imagine an array of lithographed wires on a substrate immediately beneath the cilia. In this case, we find that both the magnetic field and the magnetic field gradient may be large enough to achieve actuation. In considering the case of a lithographed wire, we will assume a gold wire of square cross section deposited on a silicon wafer. While the expressions above for magnetic field and magnetic field gradient produced by these wires are simple, the amount of current I which such wires may carry is difficult to determine. In order to arrive at a reasonable estimate, we will assume that power is delivered to the wires via resistive heating and leaves the wire via conductive losses through the silicon substrate. In the steady-state these rates are equal, thus

$$I^2 R = \frac{A}{R_T} \Delta T \tag{13}$$

where the expression on the right is Fourier's Conduction Law, in which A is the contact area between the gold and the silicon, R_T is the thermal resistance of the silicon, and ΔT is the difference in temperature between the hot wire and the cold bath below the silicon wafer. Due to the high thermal conductivity of the silicon, we will assume all conductive losses occur through the silicon and not the other three sides of the wire. In addition, we assume that the thermal resistance of the gold wire is negligible, which is valid as long as the wire is thin compared to the thickness of the silicon substrate. Rewriting the resistance in terms of the resistivity of the wire and its geometrical properties, we find that the steady-state current through the wire is given by

$$I = \sqrt{\frac{d^3}{\rho R_T}(T_H - T_C)} \tag{14}$$

where d is the width of the square cross section of the gold wire and ρ is the resistivity of the gold. Complicating matters considerably is the fact that both the resistivity of the gold and the thermal resistance of the silicon are temperature-dependent. In short, the resistivity of gold is linear with respect to temperature over a wide range ($50 \leq T \leq 1000$ K) and is given by $\rho_{Au}(T) = 8.7 \times 10^{-11} T$ Ωm (Lide, 1994). The thermal resistance is given by integrating the reciprocal of the thermal conductivity of silicon through its depth; this thermal conductivity is also dependent on temperature, and is $k_{Si}(T) = 6.83 \times 10^5 T^{-1.45}$ $Wm^{-1}K^{-1}$ for temperatures greater than 30 K (Glassbrenner & Slack, 1964). Assuming a constant thermal gradient through the silicon at steady-state and a minimal wafer thickness of 1 mm, we can find the current through the wire as a function of T_H and take the maximum. The resulting field and field gradient are plotted in Fig. 8 for wires ranging in size from 10 to 100 microns, with larger wires at the upper-left of the range and smaller wires at the lower-right. The field and gradient are sampled at a distance of 10 microns from the wire.

While no one has yet demonstrated actuation of biomimetic cilium with a current-carrying wire, the capability is enticing. However, certain considerations not yet presented must be taken into account. For example, the gradient bending calculations of Fig. 6 assume that the magnetic material is saturated; however, at the relatively low field magnitudes produced by lithographed current carrying wires, this is unlikely (see Fig. 1) and actuation will be significantly less than predicted. In addition, the direction of the gradient produced by a lithographed wire is unlikely to be optimal. Thoughtful design, however, and low-modulus, high-permeability materials may make such a system a reality.

6. Operation under a load

6.1 Introduction

Whether biological or biomimetic, an actuator may often be called upon to carry a load – to pump a fluid or to transport a bacterial plaque – and it is to such load-bearing operation that we now turn our attention. In the case of biological cilia, we will show that each cilium operates with a reserve of excess power which may be called upon to support an additional load. After tapping this reserve, the cilium operates at the expense of reduced amplitude. Magnetic biomimetic cilia have no such reserve available, and yet we show in Section 6.3 that they may be designed to operate with a robustness similar to that of their biological peers. However, in order to compare the biological to the biomimetic, we must first develop an energy model for biological cilia. In this case, energy is expended in the form of elastic energy and work done against viscous drag forces, and energy is made available through the hydrolysis of ATP.

6.2 Biological cilia
6.2.1 Elastic energy

The elastic energy of a bent cilium is shown as the first term in Equation (3), where R is the radius of curvature which in general is a function of distance along the length of the cilium. By assuming a constant curvature, we can rewrite the elastic energy in terms of the amplitude of the ciliary beat, A:

$$U_E = \frac{EI}{2L^2} A^2 \tag{15}$$

The flexural rigidity, EI, of a biological cilium has been measured in three-point bending (Okuno & Hiramoto, 1978) and stall-force experiments (Hill et al., 2010) to be approximately 7×10^{-22} Nm². A typical airway epithelial cilia is about 7 μm long and beats with a similar amplitude, yielding an elastic energy at full extension of about 1×10^{-16} J. This is in good agreement with values given for cilia of *sabellaria* and *mytilus* (Sleigh & Holwill, 1969).

6.2.2 Work done by viscous drag

The energy lost to viscous drag during the effective stroke of a cilium has previously been shown to be (Sleigh & Holwill, 1969)

$$U_D = \frac{1}{3} C_N \omega^2 L^3 t \ ; \qquad C_N = \frac{4\pi\eta}{\ln\left(\frac{2L}{d}\right) - \frac{1}{2}} \tag{16}$$

where C_N is the drag coefficient per unit length for flow normal to a cylinder.

For a 7-micron cilium of diameter 200 nm actuating in water ($\eta = 8.9 \times 10^{-4}$ Pa s), the drag coefficient is 0.0015 Pa s. The time elapsed during the effective stroke has been shown to be about 33 ms, and the drag energy is therefore approximately 2×10^{-17} J.

It is interesting to note that the energy lost to drag is an order of magnitude less than the elastic energy of a biological cilium. This tells us that the majority of the energy expenditure in a ciliary system goes toward bending the structure itself, rather than doing work on the fluid.

6.2.3 Available chemical energy

Energy for a biological cilium is provided by the hydrolysis of ATP and converted into mechanical energy by dynein, a molecular motor. To estimate the total amount of chemical energy available to a biological cilium, we may begin with the assumption that the energy available from a single dynein during the effective stroke of the cilium is given by $U_D = e_{ATP}E_{ATP}k_{ATP}t_B$, where $E_{ATP} = 1 \times 10^{-19} J$ is the chemical energy available from the hydrolysis of one ATP, e_{ATP} is the efficiency with which dynein is able to convert this chemical energy into mechanical energy, k_{ATP} is the rate of hydrolysis of ATP per dynein, and t_B is the time elapsed during one stroke. Values of k_{ATP} vary widely in the literature, but we will take 120 s^{-1} as an upper bound (Kon, Nishiura, Ohkura, Toyoshima, & Sutoh, 2004), and the time elapsed during the effective stroke of a cilium is approximately 33 ms. To arrive at a reasonable value of the conversion efficiency e_{ATP}, we note that given a stall force for a single dynein of 6 pN (Shingyoji, Higuchi, Yoshimura, Katayama, & Yanagida, 1998) and a step size of 8 nm (Holwill, 2001), the mechanical energy of a single dynein step cannot be more than the product of the two, or 4.8 x 10^{-20} J. Since this is just less than half of the chemical energy made available by the hydrolysis of ATP, the conversion efficiency e_{ATP} can be at most 0.5.

The number of dynein involved in the effective stroke of a cilium is a topic of active debate. However, most sources cite approximately 2000 outer arm dynein engaged in a 7-micron cilium (Holwill, 2001; Salathe, 2007), or a density of 2.9 x 10^8 dynein per meter. We can further refine this number by noting that since the dynein in a cilium are distributed among the nine microtubule doublets surrounding the center, not all are oriented to apply a maximum force toward the effective stroke. By geometrical considerations, we can estimate that 64% of the dynein are effective in any particular actuation[1]. The effective number of dynein involved in the ciliary beat is then $N_D = R_D n_D L$, where $R_D = 0.64$ is the fraction of dynein which are effective, $n_D = 2.9 \times 10^8$ is the number of dynein per meter, and $L = 7$ microns is the length of the cilium. The total mechanical energy available to a cilium is then the number of dynein multiplied by the energy per dynein, or

$$U_M = R_D n_D L e_{ATP} E_{ATP} k_{ATP} t_B \tag{17}$$

Using the numbers previously quoted, this total amount of chemical energy which is available for conversion to mechanical energy is about 2.6 x 10^{-16} J, which is significantly greater than the sum of elastic and drag energies for a biological cilium.

6.2.4 Beat amplitude as a function of applied load

It is interesting to note that a biological cilium has available approximately 2.6 x 10^{-16} J of useable chemical energy, yet expends only 1.2 x 10^{-16} J in a typical effective stroke. We speculate that this energy surplus is an adaptation which will allow a cilium to apply

---

[1] Given that the microtubule doublets are spaced every 40° (or 2π/9 radians) around the axis of the cilium and their component in the direction of the effective stroke is proportional to the cosine of their

angular position, the effective number of dynein can be written as $\tilde{n}_D = \dfrac{n_D}{9} \sum\limits_{n=0}^{8} \left| \cos\left(\dfrac{2\pi n}{9} \right) \right| = 0.64 n_D$

additional force in the case of an increased load. Such a load may occur due to bacterial infection or changes in the viscoelasticity of the mucus due to illness. In the case of an increased loading at the tip of the cilium, it would be reasonable to expect that the cilium is able to apply all of its available chemical energy to elastic energy and work done on the increased load: $U_M = U_E + W_L$. Here we have considered drag forces to be negligible. The work done on the load is simply the force exerted by the load multiplied by the amplitude of the ciliary beat, or $W_L = F_L A$, and so by incorporating the elastic energy term from Equation (3), we can show that the amplitude of the effective stroke under an applied loading F_L is given by

$$A = \frac{L^3}{EI}\left[\sqrt{F_L^2 + \frac{2}{L^3}EIU_M} - F_L \right] \tag{18}$$

where U_M is as described in Equation (17). The expected amplitude as a function of applied load is plotted in Fig. 9. The curved line (continued in dashes at the upper left) indicates the expected amplitude assuming all available chemical energy is used. Under normal conditions, however, a cilium works below capacity. This is indicated by the flat line at 7 microns. This reserve energy is fully expended at a load of about 30 pN, and so any additional efforts come at the expense of elastic energy and, hence, amplitude. The untapped chemical energy available an unloaded beat is given by the area of the grey box in Fig. 9.
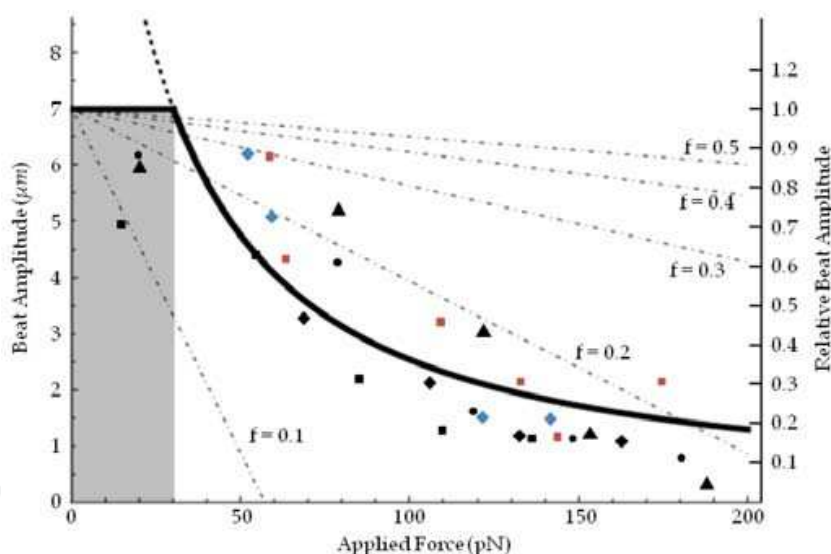

Fig. 9. Relative ciliary beat amplitude as a function of applied force at the tip of the cilium. Glyphs represent relative beat amplitude of human lung epithelial cilia taken from Hill (Hill et al., 2010). The dark black line indicates the beat amplitude of a biological cilium under an applied load predicted by Equation (18). Under 30 pN, the cilium has an additional energy reserve and beats as less than full capacity. This reserve (indicated by the area of the shaded box) is exhausted at about 30 pN. Dot-dashed lines represent relative beat amplitude of magnetic biomimetic cilia under applied load for various values of maghemite nanoparticle loading, *f*.

This prediction is in good agreement with measurements by Hill of the relative beat amplitude of human lung epithelial cilia under an applied load (Hill et al., 2010). This data is reproduced in Fig. 9 above, in which each set of glyphs represents a single cilium. Each data

set is normalized by the unloaded amplitude and represented in the original work as a relative beat amplitude (right axis).

6.3 Biomimetic cilia

In the case of field-dominated bending, we can derive an expression similar to Equation (18) for biomimetic cilia by adding the torque due to an applied load at the tip of the cilium, $\tau = F_L L$, to Equation (4). Solving for the amplitude in the case of zero net torque and normalizing with respect to unloaded beat amplitude, we find

$$A = 1 - \frac{F_L}{\frac{\pi}{4}\mu_0 M^2 f^2 r^2} \tag{19}$$

Thus, the relative decrease in amplitude with applied load is independent of the modulus of the material and depends most significantly on nanoparticle loading. Relative beat amplitudes for biomimetic cilia of biological proportions (r = 100 nm) and loaded with various volume fractions f of maghemite are represented by the dashed lines in Fig. 9. It is clear that higher loadings result in more robust cilia, and loadings as low as f = 0.2 match the load-handling capabilities of biological cilia.

7. Conclusion

We have described in this work the current state in the development of magnetically acutated biomimetic cilia, including promising candidate materials and proven fabrication techniques. In addition, we have described a predictive analytical model to aid in the design of field-generation mechanisms, materials for magnetic actuation and actuator geometry, and provide guidelines for design within the relevant parameter space. Finally, we have compared the abilities of these biomimetic cilia with that of their biological peers. While we are far from replicating the intricacies of biological cilia, the framework presented in this work will facilitate advances in the vibrant future of this field.

8. References

Alexeev, A., Yeomans, J. M., & Balazs, A. C. (2008). Designing Synthetic, Pumping Cilia That Switch the Flow Direction in Microchannels. *Langmuir, 24*(21), 12102-12106.

Antunes, M. B., & Cohen, N. A. (2007). Mucociliary clearance - a critical upper airway host defense mechanism and methods of assessment. *Current Opinion in Allergy and Clinical Immunology, 7*(1), 5-10.

Barsi, L., Buki, A., Szabo, D., & Zrinyi, M. (1996). Gels with Magnetic Properties. In *Progress in Colloid and Polymer Science* (Vol. 102, pp. 57-63). Berlin: Springer.

Bee, A., Massart, R., & Neveu, S. (1995). Synthesis of Very Fine Maghemite Particles. *Journal of Magnetism and Magnetic Materials, 149*(1-2), 6-9.

Berdichevsky, Y., Khandurina, J., Guttman, A., & Lo, Y. H. (2004). UV/ozone modification of poly(dimethylsiloxane) microfluidic channels. *Sensors and Actuators B-Chemical, 97*(2-3), 402-408.

Boucher, R. C. (2007). Cystic fibrosis: a disease of vulnerability to airway surface dehydration. *Trends in Molecular Medicine, 13*(6), 231-240.

Brumlik, C. J., Menon, V. P., & Martin, C. R. (1994). Template Synthesis of Metal Microtubule Ensembles Utilizing Chemical, Electrochemical, and Vacuum Deposition Techniques. *Journal of Materials Research, 9*(5), 1174-1183.

Cardenas-Rodriguez, M., & Badano, J. L. (2009). Ciliary Biology: Understanding the Cellular and Genetic Basis of Human Cillopathies. *American Journal of Medical Genetics Part C-Seminars in Medical Genetics, 151C*(4), 263-280.

Cartwright, J. H. E., Piro, N., Piro, O., & Tuval, I. (2008). Fluid Dynamics of Nodal Flow and Left-Right Patterning in Development. *Developmental Dynamics, 237*(12), 3477-3490.

Caykara, T., Yoruk, D., & Demirci, S. (2009). Preparation and Characterization of Poly(N-tert-butylacrylamide-co-acrylamide) Ferrogel. *Journal of Applied Polymer Science, 112*(2), 800-804.

Cebers, A. (2002). Dynamics of an elongated magnetic droplet in a rotating field. *Physical Review E, 66*(6).

Chik, H., & Xu, J. M. (2004). Nanometric superlattices: non-lithographic fabrication, materials, and prospects. *Materials Science & Engineering R-Reports, 43*(4), 103-138.

Collin, D., Auernhammer, G. K., Gavat, O., Martinoty, P., & Brand, H. R. (2003). Frozen-in magnetic order in uniaxial magnetic gels: Preparation and physical properties. *Macromolecular Rapid Communications, 24*(12), 737-741.

Downton, M. T., & Stark, H. (2009). Beating kinematics of magnetically actuated cilia. *Epl, 85*(4).

Dubois, E., Cabuil, V., Boue, F., & Perzynski, R. (1999). Structural analogy between aqueous and oily magnetic fluids. *Journal of Chemical Physics, 111*(15), 7147-7160.

Dunlop, D. J., & Ozdemir, O. (1997). *Rock Magnetism: Fundamentals and Frontiers* (1st ed.). Cambridge: Cambridge University Press.

Efimenko, K., Crowe, J. A., Manias, E., Schwark, D. W., Fischer, D. A., & Genzer, J. (2005). Rapid formation of soft hydrophilic silicone elastomer surfaces. *Polymer, 46*(22), 9329-9341.

Efimenko, K., Wallace, W., & Genzer, J. (2002). Surface Modification of Sylgard-184 Poly(dimetyl siloxane) Networks by Ultraviolet and Ultraviolet/Ozone Treatment. *Journal of Colloid and Interface Science, 254*(2), 306-315.

Evans, B. A., Shields, A. R., Carroll, R. L., Washburn, S., Falvo, M. R., & Superfine, R. (2007). Magnetically actuated nanorod arrays as biomimetic cilia. *Nano Letters, 7*(5), 1428-1434.

Fahrni, F., Prins, M. W. J., & van IJzendoorn, L. J. (2009). Magnetization and actuation of polymeric microstructures with magnetic nanoparticles for application in microfluidics. *Journal of Magnetism and Magnetic Materials, 321*(12), 1843-1850.

Fahrni, F., Prins, M. W. J., & van Ijzendoorn, L. J. (2009). Micro-fluidic actuation using magnetic artificial cilia. *Lab on a Chip, 9*(23), 3413-3421.

Ferain, E., & Legras, R. (1997). Characterisation of nanoporous particle track etched membrane. *Nuclear Instruments & Methods in Physics Research Section B-Beam Interactions with Materials and Atoms, 131*(1-4), 97-102.

Fischer, B. E., & Spohr, R. (1983). Production and Use of Nuclear Tracks - Imprinting Structure on Solids. *Reviews of Modern Physics, 55*(4), 907-948.

Fisher, J. K., Cribb, J., Desai, K. V., Vicci, L., Wilde, B., Keller, K., et al. (2006). Thin-foil magnetic force system for high-numerical-aperture microscopy. *Review of Scientific Instruments, 77*(2), 9.

Furst, E. M., Suzuki, C., Fermigier, M., & Gast, A. P. (1998). Permanently linked monodisperse paramagnetic chains. *Langmuir, 14*(26), 7334-7336.

Galicia, J. A., Sandre, O., Cousin, F., Guemghar, D., Menager, C., & Cabuil, V. (2003). Designing magnetic composite materials using aqueous magnetic fluids. *Journal of Physics-Condensed Matter, 15*(15), S1379-S1402.

Gauger, E. M., Downton, M. T., & Stark, H. (2009). Fluid transport at low Reynolds number with magnetically actuated artificial cilia. *European Physical Journal E, 28*(2), 231-242.

Glassbrenner, C. J., & Slack, G. A. (1964). THERMAL CONDUCTIVITY OF SILICON + GERMANIUM FROM 3 DEGREES K TO MELTING POINT. *Physical Review a-General Physics, 134*(4A), 1058-&.

Hill, D. B., Swaminathan, V., Estes, A., Cribb, J., O'Brien, E. T., Davis, C. W., et al. (2010). Force Generation and Dynamics of Individual Cilia under External Loading. *Biophysical Journal, 98*(1), 57-66.

Holwill, M. E. J. (2001). Dynein motor activity during ciliary beating. In M. Salathe (Ed.), *Cilia and Mucus: From Development to Respiratory Disease* (pp. 19-25). New York: Marcel Dekker.

Huczko, A. (2000). Template-based synthesis of nanomaterials. *Applied Physics a-Materials Science & Processing, 70*(4), 365-376.

Hulteen, J. C., & Martin, C. R. (1997). A general template-based method for the preparation of nanomaterials. *Journal of Materials Chemistry, 7*(7), 1075-1087.

Jolly, M. R., Carlson, J. D., Munoz, B. C., & Bullions, T. A. (1996). The magnetoviscoelastic response of elastomer composites consisting of ferrous particles embedded in a polymer matrix. *Journal of Intelligent Material Systems and Structures, 7*(6), 613-622.

Kon, T., Nishiura, M., Ohkura, R., Toyoshima, Y. Y., & Sutoh, K. (2004). Distinct functions of nucleotide-binding/hydrolysis sites in the four AAA modules of cytoplasmic dynein. *Biochemistry, 43*(35), 11266-11274.

Landau, L. D., & Lifshitz, E. M. (1986). *Theory of Elasticity, 3rd Edition*. New York: Pergamon Press.

Lide, D. R. (1994). *Handbook of Chemistry and Physics, 75th ed.*: Lewis Publishing.

Lin, C. L., Chiu, W. Y., & Don, T. M. (2006). Superparamagnetic thermoresponsive composite latex via W/O miniemulsion polymerization. *Journal of Applied Polymer Science, 100*(5), 3987-3996.

Lin, H., Watanabe, Y., Kimura, M., Hanabusa, K., & Shirai, H. (2003). Preparation of magnetic poly(vinyl alcohol) (PVA) materials by in situ synthesis of magnetite in a PVA matrix. *Journal of Applied Polymer Science, 87*(8), 1239-1247.

Makamba, H., Kim, J. H., Lim, K., Park, N., & Hahn, J. H. (2003). Surface modification of poly(dimethylsiloxane) microchannels. *Electrophoresis, 24*(21), 3607-3619.

Massart, R. (1981). Preparation of Aqueous Magnetic Liquids in Alkaline and Acidic Media. *IEEE Transactions on Magnetics, 17*(2), 1247-1248.

Massart, R., Dubois, E., Cabuil, V., & Hasmonay, E. (1995). Preparation and Properties of Monodisperse Magnetic Fluids. *Journal of Magnetism and Magnetic Materials, 149*(1-2), 1-5.

Mathur, A. M., Moorjani, S. K., & Scranton, A. B. (1996). Methods for synthesis of hydrogel networks: A review. *Journal of Macromolecular Science-Reviews in Macromolecular Chemistry and Physics, C36*(2), 405-430.

Mayer, C. R., Cabuil, V., Lalot, T., & Thouvenot, R. (2000). Magnetic nanoparticles trapped in pH 7 hydrogels as a tool to characterize the properties of the polymeric network. *Advanced Materials, 12*(6), 417-+.

McGary, P. D., Tan, L. W., Zou, J., Stadler, B. J. H., Downey, P. R., & Flatau, A. B. (2006). Magnetic nanowires for acoustic sensors (invited). *Journal of Applied Physics, 99*(8).

Mefford, O. T., Vadala, M. L., Goff, J. D., Carroll, M. R. J., Mejia-Ariza, R., Caba, B. L., et al. (2008). Stability of polydimethylsiloxane-magnetite nanoparticle dispersions against flocculation: Interparticle interactions of polydisperse materials. *Langmuir, 24*(9), 5060-5069.

Mitsumata, T., Ikeda, K., Gong, J. P., Osada, Y., Szabo, D., & Zrinyi, M. (1999). Magnetism and compressive modulus of magnetic fluid containing gels. *Journal of Applied Physics, 85*(12), 8451-8455.

Morozov, K. I., Engel, A., & Lebedev, A. V. (2002). Shape transformations in rotating ferrofluid drops. *Europhysics Letters, 58*(2), 229-235.

Nicastro, D. (2009). Cryo-Electron Microscope Tomography to Study Axonemal Organization. In *Cilia: Structure and Motility* (Vol. 91, pp. 1-39).

Okada, Y., & Hirokawa, N. (2009). Observation of Nodal Cilia Movement and Measurement of Nodal Flow. In *Cilia: Structure and Motility* (Vol. 91, pp. 265-285).

Okuno, M., & Hiramoto, Y. (1978). Direct Measurements of the Stiffness of Echinoderm Sperm Flagella. *Journal of Experimental Biology, 79*, 235-243.

Pokroy, B., Epstein, A. K., Persson-Gulda, M. C. M., & Aizenberg, J. (2009). Fabrication of Bioinspired Actuated Nanostructures with Arbitrary Geometry and Stiffness. *Advanced Materials, 21*(4), 463-+.

Qin, J., Asempah, I., Laurent, S., Fornara, A., Muller, R. N., & Muhammed, M. (2009). Injectable Superparamagnetic Ferrogels for Controlled Release of Hydrophobic Drugs. *Advanced Materials, 21*(13), 1354-1357.

Resendiz-Hernandez, P. J., Rodriguez-Fernandez, O. S., & Garcia-Cerda, L. A. (2008). *Synthesis of poly(vinyl alcohol)-magnetite ferrogel obtained by freezing-thawing technique.*

Roca-Cusachs, P., Rico, F., Martinez, E., Toset, J., Farre, R., & Navajas, D. (2005). Stability of microfabricated high aspect ratio structures in poly(dimethylsiloxane). *Langmuir, 21*(12), 5542-5548.

Rutnakornpituk, M., Thompson, M. S., Harris, L. A., Farmer, K. E., Esker, A. R., Riffle, J. S., et al. (2002). Formation of cobalt nanoparticle dispersions in the presence of polysiloxane block copolymers. *Polymer, 43*(8), 2337-2348.

Salathe, M. (2007). Regulation of mammalian ciliary beating. *Annual Review of Physiology, 69*, 401-422.

Saslawski, O., Weingarten, C., Benoit, J. P., & Couvreur, P. (1988). MAGNETICALLY RESPONSIVE MICROSPHERES FOR THE PULSED DELIVERY OF INSULIN. *Life Sciences, 42*(16), 1521-1528.

Satir, P., & Christensen, S. T. (2007). Overview of structure and function of mammalian cilia. *Annual Review of Physiology, 69*, 377-400.

Satir, P., Mitchell, D. R., & Jekely, G. (2008). HOW DID THE CILIUM EVOLVE? In *Ciliary Function in Mammalian Development* (Vol. 85, pp. 63-82).

Schonenberger, C., vanderZande, B. M. I., Fokkink, L. G. J., Henny, M., Schmid, C., Kruger, M., et al. (1997). Template synthesis of nanowires in porous polycarbonate membranes: Electrochemistry and morphology. *Journal of Physical Chemistry B, 101*(28), 5497-5505.

Shcherbakov, V. P., & Winklhofer, M. (2004). Bending of magnetic filaments under a magnetic field. *Physical Review E, 70*(6).

Shingyoji, C., Higuchi, H., Yoshimura, M., Katayama, E., & Yanagida, T. (1998). Dynein arms are oscillating force generators. *Nature, 393*(6686), 711-714.

Sidorenko, A., Krupenkin, T., Taylor, A., Fratzl, P., & Aizenberg, J. (2007). Reversible switching of hydrogel-actuated nanostructures into complex micropatterns. *Science, 315*(5811), 487-490.

Singh, H., Laibinis, P. E., & Hatton, T. A. (2005). Synthesis of flexible magnetic nanowires of permanently linked core-shell magnetic beads tethered to a glass surface patterned by microcontact printing. *Nano Letters, 5*(11), 2149-2154.

Sleigh, M. A. (1962). The Biology of Cilia and Flagella.

Sleigh, M. A., & Holwill, M. E. J. (1969). Energetics of Ciliary Movement in *Sabellaria* and *Mytilus. Journal of Experimental Biology, 50*, 733-743.

Smith, D. J., Gaffney, E. A., & Blake, J. R. (2009). Mathematical modelling of cilia-driven transport of biological fluids. *Proceedings of the Royal Society a-Mathematical Physical and Engineering Sciences, 465*(2108), 2417-2439.

Stevenson, J. P., Rutnakornpituk, M., Vadala, M., Esker, A. R., Charles, S. W., Wells, S., et al. (2001). Magnetic cobalt dispersions in poly(dimethylsiloxane) fluids. *Journal of Magnetism and Magnetic Materials, 225*(1-2), 47-58.

Stoner, E. C., Wohlfarth, E. P. (1947). A Mechanism of Magnetic Hysteresis in Heterogeneous Alloys. *Phil. Trans. of the Royal Society of London, A240*, 559-642.

Sutherland, M. J., & Ware, S. M. (2009). Disorders of Left-Right Asymmetry: Heterotaxy and Situs Inversus. *American Journal of Medical Genetics Part C-Seminars in Medical Genetics, 151C*(4), 307-317.

Szabo, D., Czako-Nagy, I., Zrinyi, M., & Vertes, A. (2000). Magnetic and Mossbauer studies of magnetite-loaded polyvinyl alcohol hydrogels. *Journal of Colloid and Interface Science, 221*(2), 166-172.

Timonen, J. V. I., Johans, C., Kontturi, K., Walther, A., Ikkala, O., & Ras, R. H. A. (2010). A Facile Template-Free Approach to Magnetodriven, Multifunctional Artificial Cilia. *Acs Applied Materials & Interfaces, 2*(8), 2226-2230.

van Ewijk, G. A., Vroege, G. J., & Philipse, A. P. (1999). Convenient preparation methods for magnetic colloids. *Journal of Magnetism and Magnetic Materials, 201*, 31-33.

Varga, Z., Feher, J., Filipcsei, G., & Zrinyi, M. (2003). *Smart nanocomposite polymer gels*.

Vilfan, M., Potocnik, A., Kavcic, B., Osterman, N., Poberaj, I., Vilfan, A., et al. (2010). Self-assembled artificial cilia. *Proceedings of the National Academy of Sciences of the United States of America, 107*(5), 1844-1847.

Wilson, K. S., Goff, J. D., Riffle, J. S., Harris, L. A., & St Pierre, T. G. (2005). Polydimethylsiloxane-magnetite nanoparticle complexes and dispersions in polysiloxane carrier fluids. *Polymers for Advanced Technologies, 16*(2-3), 200-211.

Wormuth, K. (2001). Superparamagnetic latex via inverse emulsion polymerization. *Journal of Colloid and Interface Science, 241*(2), 366-377.

Xulu, P. M., Filipcsei, G., & Zrinyi, M. (2000). Preparation and responsive properties of magnetically soft poly(N-isopropylacrylamide) gels. *Macromolecules, 33*(5), 1716-1719.

Zhang, Y., Lo, C. W., Taylor, J. A., & Yang, S. (2006). Replica molding of high-aspect-ratio polymeric nanopillar arrays with high fidelity. *Langmuir, 22*(20), 8595-8601.

Zrinyi, M., Barsi, L., & Buki, A. (1997). Ferrogel: a new magneto-controlled elastic medium. *Polymer Gels and Networks, 5*(5), 415-427.
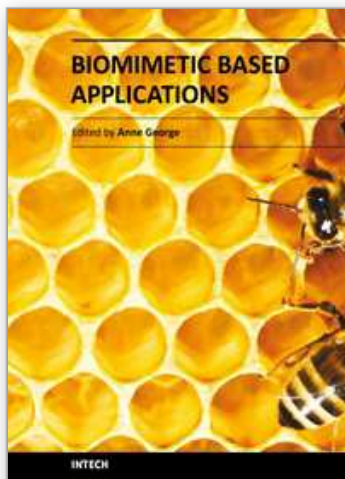
Biomimetic Based Applications

Edited by Prof. Marko Cavrak

The interaction between cells, tissues and biomaterial surfaces are the highlights of the book "Biomimetic Based Applications". In this regard the effect of nanostructures and nanotopographies and their effect on the development of a new generation of biomaterials including advanced multifunctional scaffolds for tissue engineering are discussed. The 2 volumes contain articles that cover a wide spectrum of subject matter such as different aspects of the development of scaffolds and coatings with enhanced performance and bioactivity, including investigations of material surface-cell interactions.

How to reference

In order to correctly reference this scholarly work, feel free to copy and paste the following:

Benjamin Evans and Rich Superfine (2011). Design Considerations for Magnetically Actuated Biomimetic Cilia, Biomimetic Based Applications, Prof. Marko Cavrak (Ed.), ISBN: 978-953-307-195-4, InTech, Available from: http://www.intechopen.com/books/biomimetic-based-applications/design-considerations-for-magnetically-actuated-biomimetic-cilia

INTECH
open science | open minds